IOPscience iopscience.iop.org

Home Search Collections Journals About Contact us My IOPscience

Characterization of p–n junctions of diamond and c-BN by cathodoluminescence and electron-beam-induced current

This article has been downloaded from IOPscience. Please scroll down to see the full text article.

2004 J. Phys.: Condens. Matter 16 S91

(http://iopscience.iop.org/0953-8984/16/2/011)

View the table of contents for this issue, or go to the journal homepage for more

Download details:
IP Address: 129.252.86.83
The article was downloaded on 28/05/2010 at 07:15

Please note that terms and conditions apply.

INSTITUTE OF PHYSICS PUBLISHING JOURNAL OF PHYSICS: CONDENSED MATTER

J. Phys.: Condens. Matter **16** (2004) S91–S97 PII: S0953-8984(04)66990-6

Characterization of p–n junctions of diamond and c-BN by cathodoluminescence and electron-beam-induced current

T Sekiguchi[1], **S Koizumi**[2] **and T Taniguchi**[2]

[1] Nanomaterials Laboratory, National Institute for Materials Science, Tsukuba 305-0047, Japan
[2] Advanced Materials Laboratory, National Institute for Materials Science, Tsukuba 305-0044, Japan

E-mail: Sekiguchi.takashi@nims.go.jp

Received 31 July 2003, in final form 5 November 2003
Published 22 December 2003
Online at stacks.iop.org/JPhysCM/16/S91 (DOI: 10.1088/0953-8984/16/2/011)

Abstract
p–n junctions were fabricated in diamond and cubic BN for ultraviolet light emitting diodes. These junctions were characterized by means of cathodoluminescence (CL) and electron-beam-induced current (EBIC). The line profile of CL spectra clearly revealed the different doping regions. EBIC profiles showed the band profile of these structures. The comparison of CL and EBIC results confirmed that, in both cases, the electrical fields exist at the interfaces between p and n regions. The light emitted from these structures under the current injection was compared with CL spectra from the p and n regions. It is noted that EBIC and CL are a suitable tool for the characterization of p–n junction devices of wide-gap materials with small minority carrier diffusion length.

1. Introduction

Recently, much interest has been paid to ultraviolet (UV) light for the applications of displays, lighting, photo-catalytic reactions, medical treatments etc. Because of the large size and low efficiency of UV lamps, however, these applications have been restricted to special cases so far. Thus, the development of a UV light emitting diode (LED) or laser is strongly required. Wide-gap semiconductors are the most promising materials for UV LEDs and lasers. Although UV light around 350 nm is available with the use of GaN-based materials at present, we are still on the way to development for deeper UV emitters below 300 nm. The most difficult problem in realizing such emitters is to fabricate both n and p types of wide-gap semiconductor. Since the wide-gap semiconductors are usually homopolar, much effort has been made to overcome this problem. As for diamond, for which it is difficult to fabricate an n-type layer, Koizumi *et al* [1, 2] succeeded in growing n-type films on the (111) diamond substrate by P doping.

 © 2004 IOP Publishing Ltd Printed in the UK

They have also succeeded in observing UV light emission from their diamond p–n junction [3]. However, we have to characterize this junction to determine whether this emission is yielded from the junction region or not. To diagnose this junction, we have performed electron-beam-induced-current (EBIC) and cathodoluminescence (CL) observation [4]. On the other hand, Taniguchi *et al* [5] have succeeded in fabricating p and n regions in cubic BN by Be doping. They also observed intense UV electroluminescence from this specimen. In this case, it is also necessary to characterize the junction property. In this paper, we report the EBIC and CL results of p–n junctions in diamond and c-BN and demonstrate the advantage of these methods.

2. Experimental details

Diamond p–n junctions were grown on a Ib (111) diamond substrate with 1 Ω cm resistivity and $2 \times 2 \times 0.5$ mm^3 dimensions [3]. B-doped and P-doped layers were separately grown by microwave plasma-enhanced chemical vapour deposition using a mixture of CH_3 and H_2 gas at around 900 °C. The CH_3 concentrations were 0.1% for the B-doped layer and 0.05% for the P-doped layer. Trimethylboron (TMB) and PH_3 gas diluted with hydrogen were used for B and P doping, respectively. The impurity concentrations of B and P are determined as $(1–2) \times 10^{17}$ cm^{-3} and $(7–8) \times 10^{18}$ cm^{-3}, respectively, by secondary ion mass spectroscopy. The thicknesses of B-doped and P-doped layers were about 2.0 and 1.5 μm, respectively. Then, Ar ions were implanted in the n-type layer through the mask to fabricate graphite dots with a depth of 30 nm and a diameter of 150 μm for the ohmic contact, followed by Ti and Au evaporation [6, 7]. Making use of this contact as the second mask, the outside region of implanted dots was removed by reactive ion etching to form a mesa structure using 2% CF_4 gas diluted with oxygen. The other contact was fabricated by Ti and Au evaporation at the backside of the substrate followed by annealing at 400 °C.

c-BN crystals were grown by a temperature gradient method using a mixture of Li_3BN_2 and $Ba_3B_2N_4$ as a solvent [8]. The growth condition was 5.5 GPa, 1600 °C for 20–80 h. 0.01–0.1 wt% Be was added to the solvent for p-type doping. The grown crystals have facetted faces with blue and amber colours. The former corresponded to the {111}B growth sectors, while the latter to the {111}N and {100} sectors. The secondary ion mass spectroscopy showed that the Be concentration in the blue region was about 10^{19} cm^{-3}, which was about 100 times higher than that in the amber region. Such a difference in impurity segregation with facets is often observed in the growth of polar crystals [9]. The strong segregation of Be automatically created the p–n junctions in c-BN crystals [5, 8]. For the characterization, the specimen was polished with diamond paste to reveal a fresh boundary between blue and amber regions.

Field-emission SEM equipped with an EBIC/CL system was used for the electrical and optical characterization of the p–n junction [10–12]. An electron beam of 20 kV and 1 nA was applied for both EBIC and CL observations. An electrical circuit using a battery was also used to apply bias voltage to the p–n junction from 0 to 45 V. Most of the experiments were carried out at room temperature if not otherwise stated.

3. Results and discussion

Figure 1 shows the schematic representation and secondary electron (SE) image of the diamond p–n junction diode. The p–n junction region was exposed at the side of mesa structure. The marked region in the SE image was enlarged and rotated through 90° as shown in figure 2(a). Then, the electron beam was scanned along the p–n junction region (a line in the figure) and the CL spectra were recorded as shown in figure 2(b). From these spectra we can distinguish

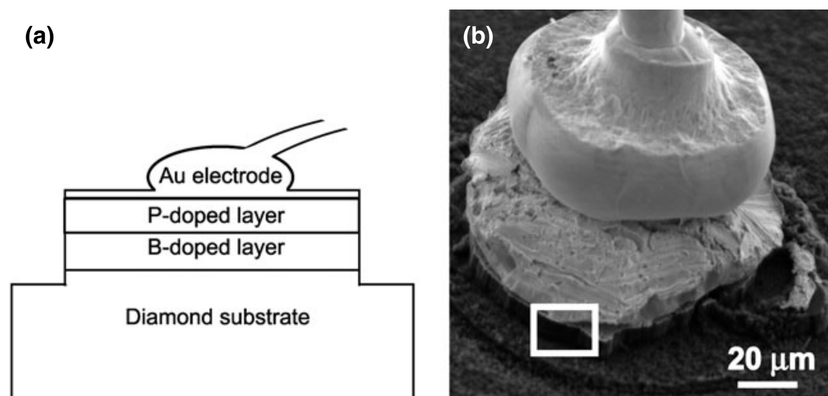

Figure 1. (a) Schematic representation and (b) secondary electron image of the p–n junction diode.

the substrate, B-doped layer and P-doped layer. The substrate did not yield any significant luminescence in the UV region. The B-doped layer yielded a weak emission at 275 nm and a broad emission at 350 nm. These emissions are attributed to the impurity-related transition [13]. The P-doped layer gave no emission in the UV region but an intense emission at 450 nm, which is the so-called band A emission related to dislocations and grain boundaries [14]. The existence of intense band A emission indicates that the P-doped layer is rather defective compared with the B-doped layer. Figure 2(c) shows the EBIC image of this region in the zero-bias condition. The bright region, that is the area where the internal electric field exists, corresponds to the interface between B-doped and P-doped layers. This indicates that the p–n junction was actually constructed at this interface. Figure 3 shows the variation of EBIC current profile against the reverse bias voltage. These curves are simulated semi-quantitatively, taking account of the dopant concentration of each layer and short carrier diffusion length. In the zero-bias condition, the depletion region was mainly spread into the B-doped layer. This phenomenon was explained using the fact that the hole concentration of the B-doped layer is about 1/40 of the electron concentration of the P-doped layer. When the reverse bias applied, the EBIC current has increased and the peak position has shifted to the B-doped region. The increase of EBIC current with the reverse bias voltage suggests that the impact ionization has occurred at the p–n junction region [15]. The existence of the peak in the EBIC profile reflects the small carrier diffusion lengths of this specimen. Namely, the minority carriers generated in the region far from the interface have difficulty in diffusing or drifting to the p–n junction, which reduces the EBIC current. Thus, the analysis of EBIC profiles gives us very important information about the p–n junction device. We should be careful, however, of the fact that EBIC observation was done under the zero- or reverse-bias condition, while the p–n LED is operated under the forward-bias condition. Figure 4 shows the electroluminescence (EL) spectrum of this diode. The comparison of the EL spectrum with the CL spectra suggests that the light emission has yielded both B-doped and P-doped layers.

As for the c-BN crystal, we have used a self-organized p–n junction. Figure 5 shows the optical micrograph of a Be-doped single crystal. The facetted faces are {111} and {100} sectors, showing the crystal symmetry. The {111}N sectors are blue, while the {111}B and {100} are amber. After the deposition of Ti/Au electrodes, direct current was applied and intense UV emission was observed at the boundary between the blue- and amber-coloured regions. Figure 6 shows the SE image and EBIC image of the polished surface of the boundary.

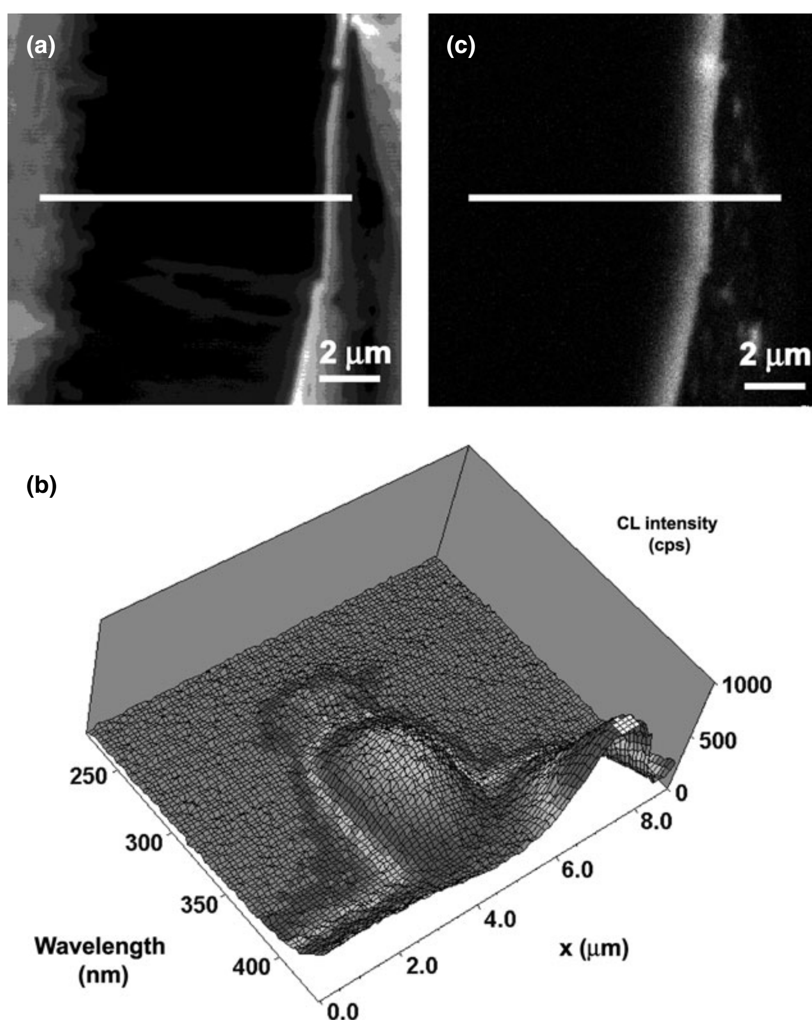

Figure 2. (a) Secondary electron image of the p–n junction region of diamond. (b) Line profile of CL spectra in the UV region along the p–n junction denoted by a bar in the SE image. (c) EBIC image at zero-bias condition.

The darker area is the polished surface and the boundary is seen at the irregular line in this area. In the EBIC image the boundary turned out to be a bright line. This is similar to the diamond case. The left-hand region, which corresponds to the blue-coloured region, is brighter than the right-hand one. It reflects the lower resistivity of this p-type region. Figure 7 shows the CL spectra of blue and amber regions as well as the EL spectra under forward- and reverse-bias conditions. Although the peak positions do not coincide with each other, we can draw the following picture. Under the forward-bias condition, defect related recombination like donor–acceptor pair transition is dominant so that the strong emission around 300 nm is yielded. The red shift of the EL emission peak might have occurred due to the applied bias voltage. Under the reverse-bias condition, on the other hand, recombination takes place simultaneously in both n-type and p-type regions so that the EL spectra become the combination of the CL spectra of n-type and p-type regions.

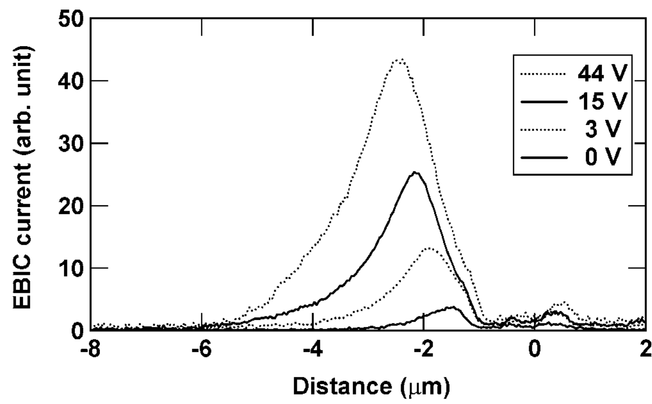

Figure 3. EBIC profiles along the diamond p–n junction under various reverse bias voltages.

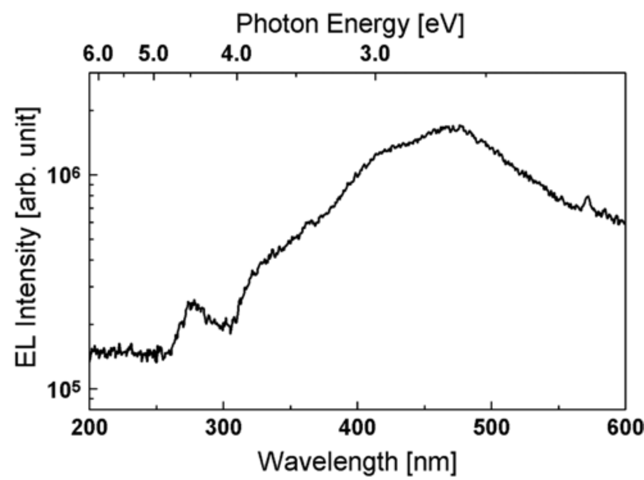

Figure 4. Electroluminescence spectrum of diamond p–n junction LED.

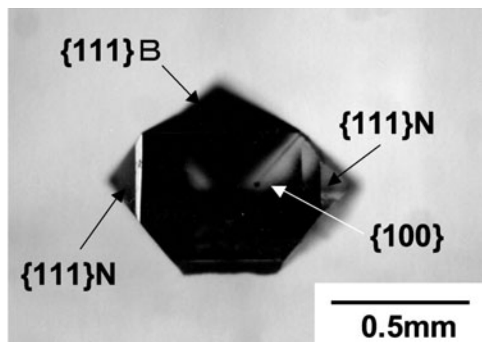

Figure 5. Optical micrograph of Be-doped c-BN.

In this study, the spatial resolution of EBIC and CL is enough to characterize these p–n junction properties. In the characterization of p–n junctions of Si, on the other hand, it is difficult to apply EBIC or CL due to the low spatial resolution resulting from long carrier

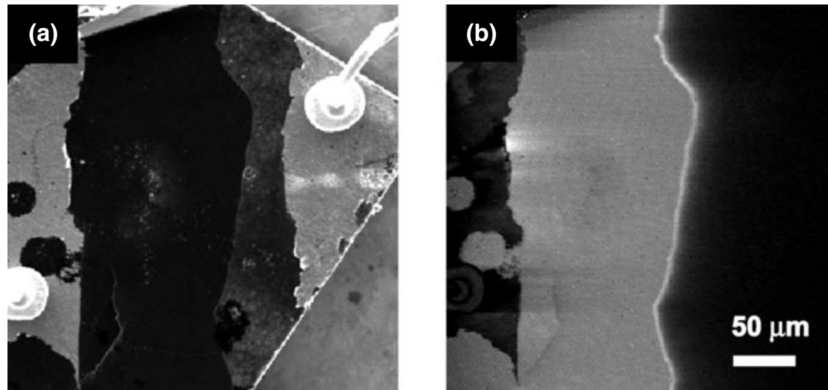

Figure 6. (a) Secondary electron image and (b) EBIC image of the p–n junction region in the c-BN crystal.

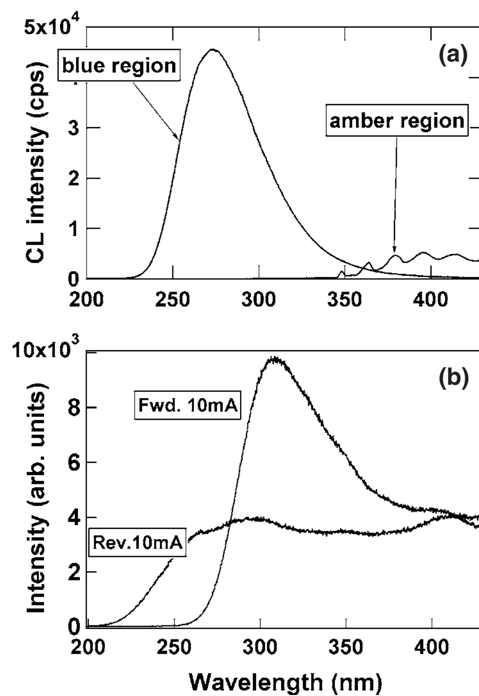

Figure 7. (a) CL spectra from blue and amber regions taken at 25 K. (b) EL spectra under forward and reverse current injections; RT.

diffusion length. The short carrier diffusion lengths in wide-gap semiconductors are favourable for these experiments to improve spatial resolution. As for c-BN, however, we have not succeeded in obtaining EBIC images under the forward- and reverse-bias conditions due to the high resistivity of the specimen. Since the wide-gap materials usually possess high resistivity that precludes the detailed EBIC experiment, we have to avoid such difficulty in some way, such as preparing the specimen in a certain geometry in which the distance between electrodes is small enough to reduce the serial resistance of the EBIC circuit. In any case, we have

found that the EBIC and CL characterization is a powerful tool to characterize the actual p–n junctions in wide-gap semiconductors.

4. Conclusion

We have characterized p–n junctions of diamond and c-BN by using CL and EBIC. Each doping layer was distinguished by the variation of CL spectra. EBIC profiles of these structures clearly showed that p–n junctions were formed at the interface between B-doped and P-doped layers in diamond and that between blue and amber regions in c-BN. EL spectra of these junctions are analysed in terms of the CL spectra of p- and n-type layers. We have emphasized the advantage of CL and EBIC for the characterization of p–n junctions in wide-gap semiconductors.

References

[1] Koizumi S, Ozaki H, Kamo M, Sato Y and Inuzuka T 1997 *Appl. Phys. Lett.* **71** 1064
[2] Koizumi S, Teraji T and Kanda H 2000 *Diamond Relat. Mater.* **9** 935
[3] Koizumi S, Watanabe K, Hasegawa M and Kanda H 2001 *Science* **292** 1899
[4] Sekiguchi T and Koizumi S 2002 *Appl. Phys. Lett.* **81** 1987
[5] Taniguchi T, Watanabe K, Koizumi S, Sakaguchi I, Sekiguchi T and Yamaoka S 2002 *Appl. Phys. Lett.* **81** 4145
[6] Prins J F 1989 *J. Phys. D: Appl. Phys.* **22** 1562
[7] Teraji T, Koizumi S and Kanda H 2000 *Appl. Phys. Lett.* **76** 1303
[8] Taniguchi T, Koizumi S, Watanabe K, Sakaguchi I, Sekiguchi T and Yamaoka S 2003 *Diamond Relat. Mater.* **12** 1098
[9] Sekiguchi T, Miyashita S, Obara K, Shishido T and Sakagami N 2000 *J. Cryst. Growth* **214** 72
[10] Sekiguchi T 2000 *Mater. Res. Soc. Symp. Proc.* **588** 75
[11] Sekiguchi T 2002 *Nano-Scale Spectroscopy and its Applications to Semiconductor Research* (*Springer Lecture Notes in Physics*) ed Y Watanabe, S Heun, G Salviati and N Yamamoto (Berlin: Springer) p 52
[12] Sekiguchi T and Sumino K 1995 *Rev. Sci. Instrum.* **66** 4277
[13] Lawson S C, Kanda H, Kiyota H, Tsutsumi T and Kawarada H 1995 *J. Appl. Phys.* **77** 1729
[14] Takeuchi D, Watanabe H, Yamanaka S, Okushi H, Sawada H, Ichinose H, Sekiguchi T and Kajimura K 2001 *Phys. Rev.* B **63** 5328
[15] Sze S M 1981 *Physics of Semiconductor Devices* (New York: Wiley) p 63